Journal of Chromatography A, 1218 (2011) 4660–4670

Contents lists available at ScienceDirect

Journal of Chromatography A

journal homepage: www.elsevier.com/locate/chroma

High-efficiency high performance liquid chromatographic analysis of red wine anthocyanins

André de Villiers[a,*], Deirdre Cabooter[b], Frédéric Lynen[c], Gert Desmet[b], Pat Sandra[c]

[a] Stellenbosch University, Department of Chemistry and Polymer Science, Private Bag X1, Matieland 7602, South Africa
[b] Vrije Universiteit Brussel, Department of Chemical Engineering (CHIS-IR), Pleinlaan 2, 1050 Brussels, Belgium
[c] Ghent University, Department of Organic Chemistry, Krijgslaan 281 S4-bis, B-9000 Ghent, Belgium

ARTICLE INFO

Article history:
Received 17 December 2010
Received in revised form 28 March 2011
Accepted 11 May 2011
Available online 18 May 2011

Keywords:
Ultra high pressure liquid chromatography (UHPLC)
High temperature liquid chromatography (HTLC)
Kinetic plots
Wine
Anthocyanins
Mass spectrometry

ABSTRACT

The analysis of anthocyanins in natural products is of significant relevance in recent times due to the recognised health benefits associated with their consumption. In red grapes and wines in particular, anthocyanins are known to contribute important properties to the sensory (colour and taste), anti-oxidant- and ageing characteristics. However, the detailed investigation of the alteration of these compounds during wine ageing is hampered by the challenges associated with the separation of grape-derived anthocyanins and their derived products. High performance liquid chromatography (HPLC) is primarily used for this purpose, often in combination with mass spectrometric (MS) detection, although conventional HPLC methods provide incomplete resolution. We have previously demonstrated how on-column inter-conversion reactions are responsible for poor chromatographic efficiency in the HPLC analysis of anthocyanins, and how an increase in temperature and decrease in particle size may improve the chromatographic performance. In the current contribution an experimental configuration for the high efficiency analysis of anthocyanins is derived using the kinetic plot method (KPM). Further, it is shown how analysis under optimal conditions, in combination with MS detection, delivers much improved separation and identification of red wine anthocyanins and their derived products. This improved analytical performance holds promise for the in-depth investigation of these influential compounds in wine during ageing.

1. Introduction

Anthocyanins (anthocyanidin-glycosides) are important natural pigments, of interest not only for their contribution to the colour of various natural products, but also in recent years due to the physiological benefits associated with their consumption. The large diversity of anthocyanin structures is associated with variations in the anthocyanidin base (18 naturally occurring anthocyanidins have been identified [1]), as well as the nature, number and position of sugars and acylated aromatic or aliphatic acids attached to each base [2,3].

Whereas many natural products are characterised by relatively simple anthocyanin profiles, red grape varieties contain a complex mixture of anthocyanins, consisting primarily of 5 anthocyanidin-glucosides and -diglucosides, as well as their acetylated and coumaroylated derivatives. During red wine production, these grape-derived anthocyanins are involved in a number of chemical transformations that play a determinative role in the sensory properties of the final product. Research conducted during the past 40 years has shed light on the most important of these chemical reactions. These include the direct [4] and acetaldehyde-mediated [5] condensation with flavanols and proanthocyanidins, the formation of anthocyanin dimers and higher oligomers [6,7], and the formation of diverse pyranoanthocyanins through the reaction of anthocyanins and acetaldehyde [8], pyruvic acid [9,10], cinnamic acids (in particular, coumaric-, ferulic-, caffeic- and synapic acids) [11,12], acetoacetic acid [13] and procyanidins in the presence of acetaldehyde [14,15]. Moreover, anthocyanin–pyruvic acid adducts have been shown to react with flavanols in the presence of acetaldehyde to produce so-called portisins [16]. As these derived pigments progressively replace grape-derived anthocyanins during wine maturation, they become influential in determining the colour, and to some extent through their incorporation in the tannin structure, the taste properties of aged red wine.

Clearly, the analytical determination of anthocyanins and their derived products in red wine is of importance to the wine industry. At the same time, the large numbers and sheer diversity of red wine anthocyanins hampers their separation and quantification. Reversed phase liquid chromatography (RP-LC) is by far the most common analytical method used for the characterisation of

* Corresponding author. Tel.: +27 021 808 3351; fax: +27 021 808 3360.
E-mail address: ajdevill@sun.ac.za (A. de Villiers).

0021-9673/$ – see front matter © 2011 Elsevier B.V. All rights reserved.
doi:10.1016/j.chroma.2011.05.042

red wine pigment fractions. Although anthocyanin separations on a mixed mode phase can improve the selectivity, the efficiency decreases with such a stationary phase [17]. Selective UV detection in the range 500–550 nm may be used to detect these molecules, although mass spectrometric (MS) detection is increasingly being used due to the inherent power of LC–MS for structural elucidation purposes. However, despite the well-documented benefits of MS detection for anthocyanin determination, the similarity of red wine pigments, coupled to the fact that complete separation of the target analytes cannot be achieved using conventional RP-LC methods, complicates their identification and quantification. As a result, complex pre-fractionation procedures are often used to facilitate the identification of low-level anthocyanin-related compounds [18].

Our own research [19] aimed at improving the HPLC analysis of anthocyanins has indicated that conventional RP-LC inherently suffers from poor chromatographic efficiency, resulting in less-than-optimal resolution. We have shown that the slow (i.e. occurring on the time-scale of chromatographic separations) interconversion between carboninol-pseudobase and flavylium cationic species in solution is the cause of excessive band broadening under conventional RP-LC conditions [19]. We further demonstrated that elevated temperature in combination with small particle-packed columns may be used to circumvent these inherent limitations.

Here we report the development of an optimal RP-LC method for anthocyanin determination, taking into account the precedent considerations. In order to arrive at optimal experimental conditions, chromatographic data for malvidin-3-O-glucoside, the principal red wine anthocyanin, were used to construct kinetic plots. Kinetic plots represent a powerful family of representation techniques that may be used to derive optimal conditions for a given separation problem in terms of the compromise between analysis time and required efficiency [20]. Importantly, the use of experimental data implies that the results may be accurately extrapolated to provide information on the best experimental conditions for the analysis of a given analyte [21].

We therefore used measured plate height data for malvidin-3-O-glucoside to derive optimal experimental conditions for the analysis of red wine anthocyanins on conventional HPLC instrumentation, taking into consideration practical constraints of analysis time, column length and mobile phase flow rate. We further demonstrate the benefits of the proposed optimal conditions for the gradient RP-LC analysis of red wine anthocyanins, using both UV and MS detection, and highlight the benefit in resolution obtained using these conditions.

2. Experimental

2.1. Materials

Uracil (98%), HPLC grade acetonitrile and formic acid were from Sigma–Aldrich (Atlasville, South Africa) and LC–MS grade acetonitrile from Romil (Cambridge, UK). Deionised water was obtained from a Milli-Q purification system (Millipore, Milford, MA, USA). Malvidin-3-glucoside chloride (MVG, Oenin chloride) was obtained from Extrasynthese (Genay, France), and dissolved at 1 mg/mL in methanol as stock solution. 2-year old Pinotage wine samples used in this study were obtained from the South African Young Wine show and the Institute for Wine Biotechnology (Stellenbosch University, South Africa). Wine samples were filtered (0.45 μm HV, Millipore) prior to analysis.

The following columns from Waters (Milford, MA, USA) were used: Acquity BEH C18 (2.1 mm I.D. × 100 mm L, 1.7 μm d_p) and XBridge C18 (4.6 mm I.D. × 250 mm L, 5 μm d_p).

2.2. Instrumentation

HPLC-UV analyses were performed on an Acquity UPLC system equipped with a binary solvent manager, sample manager, column manager and photodiode array (PDA) detector equipped with a 500 nL flow cell (10 mm path length) (Waters).

LC–MS analyses were performed on a UPLC system equipped with a binary solvent manager, autosampler and column heater, coupled via an electrospray ionisation (ESI) source to an API Q-TOF Ultima time-of-flight (TOF) mass spectrometer (Waters). A capillary voltage of +3.5 kV and a cone voltage of 35 V were applied using a source temperature of 100 °C and a desolvation temperature of 350 °C. The desolvation and cone gas flows (both N_2) were 400 L/h and 50 L/h, respectively. The mass spectrometer was operated in positive ionisation mode. For analyses on the XBridge column, the eluate from the UPLC system was split 1:4 prior to introduction into the ionisation chamber. Masses were scanned from 200 to 1500 amu and data were collected and processed using MassLynx v.4.0 software (Waters). The instrument was calibrated with sodium formate solution. Since no lock-spray function was available on this instrument, m/z ratios are reported in unit mass resolution.

2.3. Chromatographic conditions

2.3.1. Construction of van Deemter curves

Van Deemter curves for malvidin-3-O-glucoside (MVG) were constructed according to the procedure outlined elsewhere [19]. Briefly, an Acquity BEH C18 column (100 mm × 2.1 mm, 1.7 μm) was used together with mobile phases consisting of 7.5% (v/v) formic acid in water (A) and 7.5% (v/v) formic acid in acetonitrile (B). The mobile phase composition was 90/10 (phase A/phase B) for experiments conducted at 25 °C, and 92/8 at 50 °C, and the injection volume 1.8 μL. The retention factor, k, for MVG under these conditions was ~5. Detection was performed at 280 and 500 nm using data acquisition rates sufficient to provide minimum 20 data points per peak. The sample contained 20 mg/L uracil and 50 mg/L malvidin-glucoside dissolved in 10% MeOH and 90% mobile phase A.

2.3.2. UHPLC-PDA and UHPLC-PDA–MS gradient analysis

The mobile phases for all gradient analysis consisted of 7.5% (v/v) formic acid in water (A) and 7.5% (v/v) formic acid in acetonitrile (B), respectively. Analyses on the XBridge column were performed using the following elution conditions at a flow rate of 1 mL/min: 0–1 min 1%B, 1–12 min 1–13.5%B, 12–24 min 13.5–23.5%B, 24–28 min 23.5–28.5%B, 28–35 min 28.5%B (re-equilibration 10 min). The column was thermostatted to 25 °C, UV detection was performed at 500 nm (10 Hz), and 10 μL of the filtered wine sample was injected in partial loop with needle overfill mode (4 μL was injected for MS analyses).

UPLC gradient analyses were performed on two 100 mm columns coupled in series using 1.8 μL stainless steel tubing. Analysis was performed at 50 °C using a flow rate of 0.06 mL/min and the following gradient: 0–3 min 1%B, 3–34 min 1–13.5%B, 34–67 min 13.5–23.5%B, 67–78 min 23.5–28.5%B, 78–98 min 28.5%B (re-equilibration 15 min). UV detection was performed at 500 nm (10 Hz) and 5 μL was injected in partial loop with needle overfill mode (4 μL was injected for MS analyses).

2.4. Data analysis and construction of kinetic plots

All values represent the average of at least duplicate measurements. Theoretical plates (N) for the construction of Knox curves were calculated using the peak width at half height obtained from Chemstation software (Agilent Technologies, Waldbronn,

Germany), while the retention time of uracil (t_0) was used to calculate the linear velocity u_0 (mm/s) [19].

Kinetic plots were constructed using a freely downloadable spreadsheet template [20]. The mobile phase viscosity (η, Pa s) was calculated according to Chen and Horváth [22] (using water/acetonitrile for the buffered phases). Diffusion coefficients (D_m) in m^2/s were calculated using the Wilke–Chang equation [23]. Column permeabilities (K_v in m^2) were determined using the following relation [24]:

$$K_v = \frac{u_0 \eta L}{\Delta P} \quad (1)$$

in which ΔP is the pressure drop (in $Pa = N/m^2$) over the column with length L (m). The column pressure drop and the linear velocity u_0 were obtained after correction for the system contributions under identical conditions. Permeability measurements were performed at low flow rates (0.05 mL/min for the 2.1 mm I.D. columns and 0.5 mL/min for the 4.6 mm I.D. columns) to minimise measurement errors due to changes in viscosity and temperature at high pressures [25].

Experimental values for the retention factors of all compounds were obtained using Empower software (Waters). These values were obtained at low linear velocities to avoid changes in retention factor as a function of column pressure. As reference lengths the nominal particle size specified by the column manufacturer (i.e. 1.7 and 5 μm) were used. Values 400 and 1000 bar for the maximum pressure were used for the XBridge and Acquity columns, respectively.

3. Results and discussion

3.1. Evaluation of optimal experimental conditions for anthocyanin analysis using kinetic plots

In a precedent report [19] we demonstrated that generic RP-LC methods for anthocyanin analysis are performed far from the optimal conditions for maximum chromatographic efficiency. We further demonstrated that exceptionally low optimal linear velocities – and significant efficiency-loss at high velocities – are the result of band broadening due to the slow interconversion between flavylium cationic and carbinol pseudobasic forms of anthocyanins. Two complementary ways to improve the chromatographic separation of anthocyanins were therefore explored. First, faster mass transfer provided by small particles was shown to improve chromatographic efficiency, while simultaneously increasing the optimal linear velocity. It was however noted that, in order to benefit from the advantages of small particles, a relatively long column should be employed due to the dependence of the effect of secondary equilibria on the absolute retention time. Secondly, temperatures up to 50 °C were used to increase the rate of important secondary equilibria reactions, leading to flatter van Deemter curves and a further increase in efficiency. We have shown that thermal degradation of anthocyanins does not pose a problem under these conditions [19].

However, practically relevant information such as the optimal particle size/column length/temperature/pressure combination is less straightforward to deduce from plate height curves such as reported previously [19]. Therefore, in order to evaluate the most favourable experimental configuration for high-efficiency anthocyanin determination, experimental plate height data for each column were used to construct kinetic plots. This was done by combining height equivalent to a theoretical plate (H) and linear velocity (u_0) values with experimentally determined permeability data, mobile phase viscosity and maximum instrument pressure (see Section 2.4 for details) using the following equations [20]:

$$t_0 = \left(\frac{\Delta P}{\eta}\right)\left[\frac{K_v}{u_0^2}\right]_{exp} \quad (2)$$

$$N = \left(\frac{\Delta P}{\eta}\right)\left[\frac{K_v}{u_0 H}\right]_{exp} \quad (3)$$

Subsequently using:

$$t_R = t_0(1 + k) \quad (4)$$

where k is the retention factor, turns each point of the original van Deemter curve into a data point that relates a given efficiency (N) to the analysis time (t_R) needed to achieve it on a column with a length limited by the pressure drop and filled with the particle type under consideration. This type of plot is preferred because it yields the most relevant information for the optimization of complex anthocyanin analysis.

A supplementary feature of the kinetic plot program allows addition of practical constraints [26]. These constraints can be used to avoid those parts of the plots corresponding to solutions which are difficult to realize in practice. For example a constraint can be put on the column length (by defining a maximum or minimum column length) to avoid data points relating to impractically large or short column lengths. Furthermore, by setting an equal upper- and lower limit for the column length, a kinetic plot is obtained that is valid for a fixed column length. This hence allows to extrapolate the kinetic performance obtained on a column with a given length to an equally well-packed column with a different length. This approach was used to extrapolate the efficiency obtained for MVG on the 1.7 μm and the 5 μm columns of 100 and 250 mm in length, respectively, to fixed length kinetic plot curves. A length of 250 mm was selected for the 5 μm phase as this represents the most common column length for conventional RP-LC analyses of anthocyanins. A length of 200 mm was used for the UHPLC column, as it was shown previously [19] that the benefits of 1.7 μm columns can only be exploited without significant reduction in column length. Moreover, as will be demonstrated further, gradient analysis using this length is easily achievable on conventional instrumentation. In this way, experimental data were used to investigate the effect of switching to a smaller particle size and a higher operating temperature on the isocratic efficiency. Fig. 1 shows the constrained kinetic plots for these two columns at 25 °C.

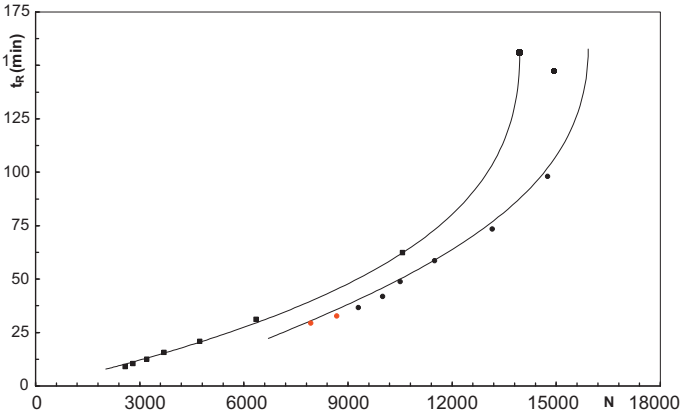

Fig. 1. Constrained kinetic plots of analysis time (t_R) versus efficiency (N) for malvidin-3-glucoside (MVG) on an Acquity 1.7 μm column with a fixed length of 200 mm (•) and an Xbridge 5 μm column with a fixed length of 250 mm (■). Temperature: 25 °C, mobile phase: 7.5% (v/v) formic acid in water/7.5% (v/v) formic acid in acetonitrile (90:10, v/v). Red points correspond to operation at pressures above 400 bar. (For interpretation of the references to colour in this figure legend, the reader is referred to the web version of the article.)

In contrast to a "normal" free kinetic plot (without constraints), where every data point relates to a column of different length operated at the maximum pressure, and hence operated at a different chromatographic velocity, every data point in a constrained kinetic plot corresponds to the same column length now operated at a different pressure in order to change the linear velocity. In Fig. 1 the data points corresponding to the longest analysis times (the upper part of the plot) are operated at the lowest pressures and velocities. The data points corresponding with the shortest analysis times correspondingly agree with columns operated at high pressures and high velocities. From Fig. 1 it is clear that for both columns, a higher efficiency is reached at low velocity. This is due to the fact that at low velocities, the plate height contribution due to secondary equilibria (specifically the hydration reaction) becomes less influential [19]. The analysis time will decrease significantly when increasing the pressure, but this will be accompanied by a decrease in efficiency. Furthermore, the 1.7 μm column, in its present length of 200 mm, will yield a slightly higher efficiency than the 5 μm column of 250 mm for a given analysis time, both at high and low velocity and hence over the entire range of available pressures. Alternatively, the same chromatographic efficiency may be obtained in a shorter analysis time using the 1.7 μm column. Moreover, the maximum efficiency achievable on the 200 mm 1.7 μm column is higher than for the 250 mm 5 μm column (although both values are still significantly lower than expected based on the $H_{min} \sim 2d_p$ criterion considered the norm for normal analytes).

Because of its higher flow resistance, the 1.7 μm column, however, requires a pressure in excess of 400 bar (1000 bar for the fastest analysis) for analysis times below ~35 min. As can be seen from the plot, increasing the pressure beyond 400 bar will improve speed at the cost of efficiency. This is due to the fact that the selected column lengths are both optimally exploited at much lower pressures as a result of the low optimal velocity observed for anthocyanins.

Constrained kinetic plots were subsequently constructed for the data obtained on the 1.7 μm column at 25 and 50 °C. It was previously demonstrated that a moderate increase in temperature has an especially beneficial effect on the plate-height curves for MVG, due to faster kinetics of the hydration reaction [19]. In Fig. 2 the column length was again fixed at 200 mm.

Again, there is a clear increase in efficiency when operating the column at low velocity (and hence long analysis times) both at low and high temperature. At both temperatures an increase in maximum pressure will only provide a benefit for fast, low-efficiency analyses. Increasing the temperature leads to a significant improvement in efficiency, resulting from faster mass transfer on the one hand and decreased band-broadening due to secondary equilibria on the other hand. For example, for an analysis time of 40 min an increase in efficiency from 9500 to 17,000 plates is observed at 50 °C compared to 25 °C. Similar gains are observed for analysis times <60 min. For longer analysis times, the efficiency at 50 °C will start decreasing slightly. In contrast, the efficiency at 25 °C increases to a maximum value of $N \approx 15{,}000$ at 150 min, which nevertheless remains lower than the maximum efficiency of $N \approx 18{,}000$ at 50 °C (obtained for analysis times of ~45 min). This observation can be ascribed to the higher optimal velocity observed for MVG at the latter temperature, which leads to an earlier (in terms of t_R) onset of B-term band-broadening.

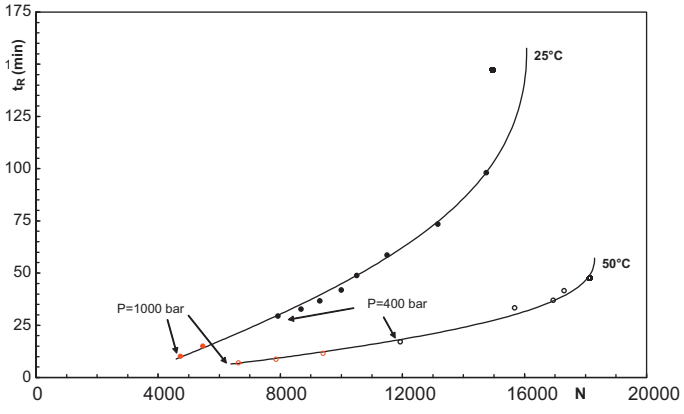

Fig. 2. Constrained kinetic plots of analysis time (t_R) versus efficiency (N) for malvidin-3-glucoside (MVG) on an Acquity 1.7 μm column with a fixed length of 200 mm at 25 °C (•) and 50 °C (○). Mobile phase: 7.5% (v/v) formic acid in water/7.5% (v/v) formic acid in acetonitrile (90:10, v/v) for 25 °C and (92:8, v/v) for 50 °C. Red points correspond to operation at pressures above 400 bar. (For interpretation of the references to colour in this figure legend, the reader is referred to the web version of the article.)

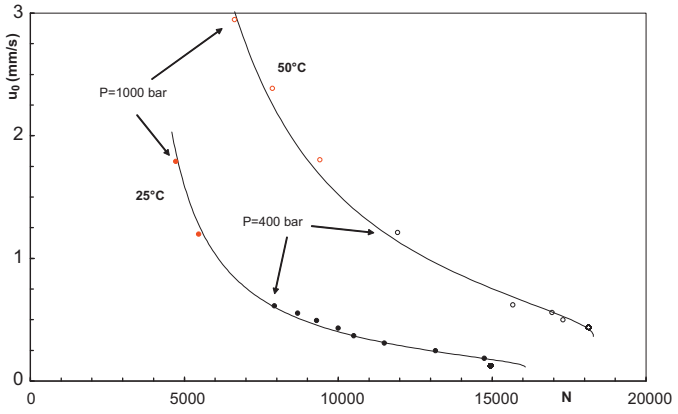

Fig. 3. Constrained kinetic plots of linear velocity (u_0) versus efficiency (N) for malvidin-3-glucoside (MVG) on an Acquity 1.7 μm column with a fixed length of 200 mm at 25 °C (•) and at 50 °C (○). Experimental conditions are the same as in Fig. 2. Red points correspond to operation at pressures above 400 bar. (For interpretation of the references to colour in this figure legend, the reader is referred to the web version of the article.)

To obtain the flow rate or velocity at which the system should be operated to reach the highest efficiency, the plot of t_R versus N can be converted to a plot of u_0 versus N by rearranging the y-axis according to:

$$u_0 = \frac{L(1+k)}{t_R} \tag{5}$$

Fig. 3 shows the constrained kinetic plot of u_0 versus N for the 1.7 μm at 25 °C and at 50 °C. As was already clear from Fig. 2, the highest efficiency is reached at the lowest velocity, 0.12 mm/s at 25 °C and 0.37 mm/s at 50 °C. These values may be translated to volumetric flow rates (F) using:

$$F = \frac{\pi d_c^2}{4} u_0 \varepsilon_t \tag{6}$$

where d_c is the column diameter and ε_t the total porosity. For the 2.1 mm I.D. columns used here, u_{opt} values at 25 and 50 °C correspond to flow rates of 0.02 mL/min and 0.06 mL/min, respectively. Of course, these efficiencies will only be reached for long analysis times. This is especially true at 25 °C, although it should be remembered that 1.7 μm columns provide faster analyses than 5 μm phases (Fig. 1). The compromise between slow, high efficiency analysis and fast, low efficiency analysis is therefore of particular importance in the case of anthocyanin analyses, and in fact an increase in temperature generally shifts chromatographic performance to more acceptable ranges in terms of both parameters.

It should be noted that the dependence of plate height behaviour on column length stemming from slow secondary equilibria has implications for the accuracy of the kinetic plot data. For the con-

struction of kinetic plots, it is assumed that H varies with u_0 in a manner which is independent of L. While this is demonstrably the case for most analytes, this assumption no longer holds true in the case of anthocyanins. For this reason, fixed-length constrained kinetic plots should be used to evaluate anthocyanin separations. The kinetic plots shown in this sections should therefore merely be considered as a qualitative reflection of the effects that can be expected when changing the particle size and operating temperature for anthocyanin analysis using a given column length, rather than an accurate qualitative prediction for all column lengths.

3.2. Proposed optimized HPLC analysis of wine anthocyanins

Clearly, better performance for the HPLC separation of anthocyanins is obtained when using low linear velocities on long columns packed with small particles and operated at above-ambient temperature. Note that the effect of temperature should apply equally to larger particle sizes, although the lower optimal linear velocities on 5 μm phases would lead to impractically long analyses.

Although the precedent data clearly demonstrate the significant effect of the inter-species conversion on the isocratic efficiency of anthocyanin separations, the question remains to what extent these observations will affect the quality of gradient elution separations. These separations are commonly evaluated in terms of peak capacity, a term used to describe the number of compounds that could (ideally) be separated with unity resolution under gradient conditions. According to Wang et al. [27], the optimization of peak capacity in gradient elution is equivalent to plate count optimization in isocratic elution, on condition that in optimizing peak capacity by varying column length or particle size, the gradient steepness is held constant. In practice this implies keeping the ratio of the gradient time (t_G) to the void time (t_0) constant between the columns. This means that all conclusions drawn from isocratic plate count optimization with kinetic plots should in principle be applicable to peak capacity optimization in gradient elution. This has recently been confirmed, even for cases with important peak compression, in a mathematically rigorous way [28].

To demonstrate that the qualitative predictions obtained from the isocratic kinetic plots are equally applicable under gradient conditions, isocratic and gradient peak capacities were calculated for the analysis of a red wine sample using: (i) typical conditions for anthocyanin analysis (250 mm × 4.6 mm 5 μm column, 25 °C and a flow rate of 1 mL/min) and (ii) optimal analysis conditions on a 200 mm 1.7 μm column operated at 50 °C and 0.06 mL/min flow rate.

The linear velocity at 1 mL/min is ~1.7 mm/s on the 5 μm XBridge column. From the kinetic plot data, this corresponds to an isocratic efficiency of 4700 plates on the 5 μm XBridge column. For the 1.7 μm column, $N \sim 18{,}200$ under the optimal conditions used here (i.e. a ~3.9× increase in isocratic efficiency). These values may be translated to isocratic peak capacities ($n_{p(i)}$) using the following relation [29]:

$$n_{p(i)} = \frac{\sqrt{N}}{4} \ln(1+k) + 1 \quad (7)$$

Isocratic peak capacities of 32 and 61 are calculated for conventional and optimal analyses of MVG using these data (i.e. an increase of a factor 1.9×, corresponding well with the 3.9× increase in efficiency, since $n_{p(i)} \sim \sqrt{N}$). For the calculation of gradient peak capacities, the relation derived by Neue was used [30]:

$$n_p = 1 + \frac{t_G}{(1/n)\sum_1^n w} \quad (8)$$

where n is the number of peaks selected for the calculation of the peak capacity, w is the width of the peak at the base (4σ) and t_G is the gradient run time. RP-LC-UV chromatograms for each of these separations are shown in Fig. 4. The gradient run times were adjusted in each case to maintain the same gradient steepness. 15 peaks were selected, representing both less- and well retained compounds (a necessary condition to get an accurate representation of the peak capacity) to calculate the peak capacity according to Eq. (8). Note that most of the peaks selected correspond to the major grape-derived anthocyanins, compounds which are expected to be most susceptible to band-broadening due to secondary equilibria. Nevertheless, as these represent the most abundant species in most wines, this selection reflects accurately the separation power for wine analysis.

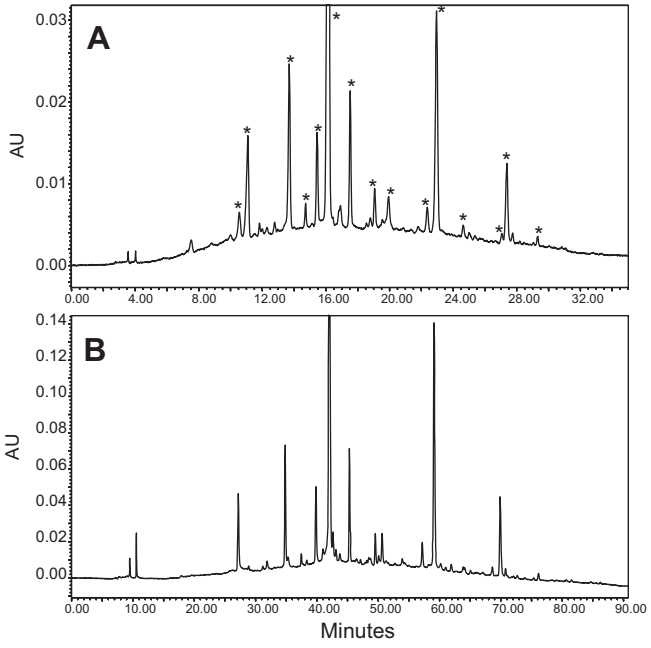

Fig. 4. Gradient analysis of a Pinotage wine sample: (A) 1 mL/min (ΔP_{max} = 220 bar), 25 °C on an Xbridge C18 column (250 mm L × 4.6 mm I.D., 5.0 μm d_p); (B) 0.06 mL/min at 50 °C (ΔP_{max} = 149 bar), on Acquity BEH C18 columns (2 mm × 100 mm L × 2.1 mm I.D., 1.7 μm d_p). Detection: UV, 500 nm. * denotes peaks used to calculate the peak capacity. For further experimental details, refer to Section 2.3.2.

Analysis under conventional conditions provided a peak capacity of 159, a value which is increased to 287 on the 1.7 μm column operated at 50 °C and optimal flow rate (optimal conditions). This gain (by a factor 1.8×) corresponds well with the calculated gain in isocratic peak capacity by a factor 1.9×. This important increase in peak capacity by reduction in flow rate is clearly evident upon investigation of Fig. 4, and follows directly from the abnormal plate height behaviour of MVG [19]. Therefore the improved efficiency

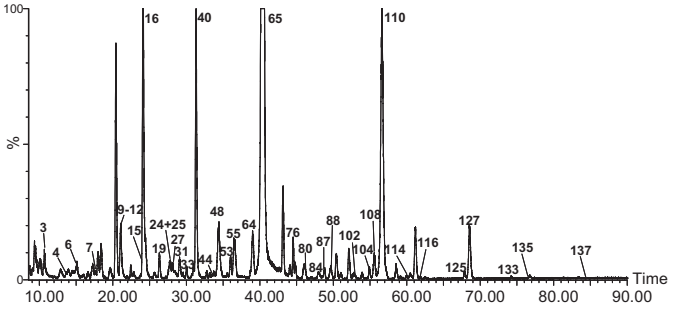

Fig. 5. TIC for the UHPLC–ESI-MS analysis of a Pinotage wine sample under optimal conditions. Experimental conditions as specified in Fig. 4b and Section 2.3.2. Peak numbers correspond to Tables 1–4.

Table 1
Anthocyanidin-glucosides, -di-glucosides and oligomeric anthocyanins tentatively identified in a 2-year old Pinotage wine. Peak numbers correspond to Figs. 5–8.

Peak No.	t_R (min)	M+	Compound[a]	Reference(s)
Anthocyanidin-glucosides				
25	27.80	465	Delphinidin-3-glucoside (Dp-glc)	[30,31,47]
42	32.40	449	Cyanidin-3-glucoside (Cy-glc)	[30,31,47]
48	34.44	479	Petunidin-3-glucoside (Pt-glc)	[30,31,47]
51	35.58	493	Malvidin-3-galactoside	[32]
64	39.02	463	Peonidin-3-glucoside (Pe-glc)	[30,47]
65	40.38	493	Malvidin-3-glucoside (Mv-glc)	[30,31,47]
72	42.97	507	Delphinidin-3-acetylglucoside (Dp-acetylglc)	[30,31,47]
81	46.97	535	Malvidin-3-acetylgalactoside	[32]
84	48.03	491	Cyanidin-3-acetylglucoside (Cy-acetylglc)	[30,31,47]
88	49.63	521	Petunidin-3-acetylglucoside (Pt-acetylglc)	[30,31,47]
106	55.14	611	Delphinidin-3-(p-coumaroyl)glucoside (Dp-coumglc)	[30,31]
108	55.58	505	Peonidin-3-acetylglucoside (Pe-acetylglc)	[31,47]
110	56.59	535	Malvidin-3-acetylglucoside (Mv-acetylglc)	[30,31,47]
115	60.12	655	Malvidin-3-(caffeoyl)-glucoside	[30,47]
116	61.86	625	Petunidin-3-(p-coumaroyl)glucoside (Pt-coumglc)	[30]
121	64.93	639	Malvidin-3-(p-coumaroyl)glucoside *cis*	[30,31]
125	67.86	609	Peonidin-3-(p-coumaroyl)glucoside (Pe-coumglc)	[30,47]
127	68.54	639	Malvidin-3-(p-coumaroyl)glucoside *trans* (Mv-coumglc)	[30,31]
Anthocyanidin-di-glucosides				
10	21.15	627	Dp-3,5-diglucoside	[33]
33	30.03	625	Pe-3,5-diglucoside	[34]
38	31.00	655	Mv-3,5-diglucoside	[30,33]
52	35.70	625	Pe-3,7-diglucoside	[30]
58	37.10	655	Mv-3,7-diglucoside	[30]
111	57.25	801	Mv-3-coumaroyl-5-diglucoside	[33]
Oligomeric anthocyanins				
30	28.54	1273	(epi)catechin-Mv-glc-Mv-glc[b]	[6,48]
69	41.92	957	Mv-Dp-2glc dimer	[6,7,48]
75	44.52	971	Mv-Pt-2glc dimer	[6,7,48]
98	51.89	955	Mv-Pe-2glc dimer	[6,7,48]
99	52.13	985	Mv-Mv-2glc dimer	[6,7,48]
112	59.56	1027	Mv-glc-Mv-acetylglc dimer	[48]
119	63.77	1131	Mv-glc-Mv-coumglc dimer	[6,7,36,48]

[a] Dp = delphinidin, Cy = cyanidin, Pt = petunidin, Pe = peonidin, Mv = malvidin, glc = glucoside, coum = coumaroyl-.
[b] Identification of proanthocyanin isomer could not be established due to lack of standards.

observed for low flow rates under isocratic conditions clearly translates into higher peak capacities under gradient conditions at the same flow rates.

Comparing the peak capacities obtained on the 1.7 μm and 5 μm columns we can conclude that a large increase in peak capacity is observed by switching to (1) a smaller particle size, (2) a lower flow rate and (3) a higher temperature. Furthermore, these results indicate that the qualitative predictions made from the kinetic plots, obtained from isocratic band-broadening data for the main wine anthocyanin, malvidin-3-O-glucoside, can indeed be used to optimize the gradient analysis of wine anthocyanins.

3.3. LC–MS analysis of red wine anthocyanins under optimal conditions

High-efficiency HPLC analysis in combination with MS detection shows particular promise for the detailed investigation of complex natural pigment fractions such as encountered in red wine. Since many of the anthocyanin-derived pigments are present in relatively low amounts and co-elution with grape-derived anthocyanins is inevitable using conventional routine RP-LC methods, this approach would greatly facilitate the identification of minor constituents using a generic LC–MS screening method. An example of the optimized gradient UHPLC–MS analysis of a red wine sample on 2 mm × 100 mm 1.7 μm columns is shown in Fig. 5 (peak numbers in this figure correspond to Tables 1–4). Extracted ion chromatograms highlight the improved separation of selected anthocyanins compared to HPLC–MS analysis of the same wine sample under conventional conditions (a 5 μm 250 mm × 4.6 mm column operated at 25 °C and 1 mL/min) in Figs. 6 and 7. While analysis time for the optimized UHPLC–MS method is more than

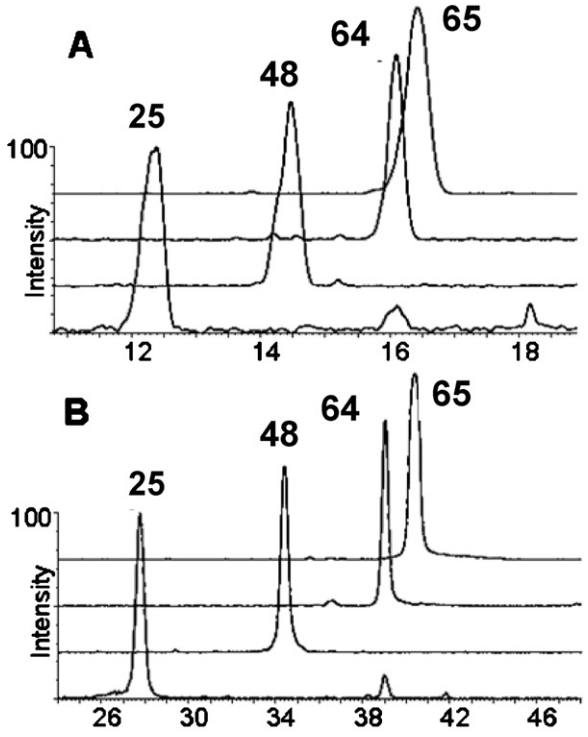

Fig. 6. Comparison of extracted ion chromatograms for the analysis of anthocyanidin-glucosides in red wine under conventional (A: 250 mm L × 4.6 mm I.D., 5 μm d_p column, 25 °C, 1 mL/min) and optimized conditions (B: 2 mm × 100 mm L × 2.1 mm I.D., 1.7 μm d_p column, 50 °C, 0.06 mL/min). Peak numbers correspond to Table 1.

Table 2
Anthocyanin-proanthocyanin derived products tentatively identified in a 2-year old Pinotage wine. Peak numbers correspond to Figs. 5–8.

Peak No.	t_R (min)	[M+]	Compound[a]	Reference(s)
Direct anthocyanin–tannin adducts				
8	18.52	797	Mv-glc-(epi)gallocatechin (T–A type)[b]	[38]
14	24.00	767	Pt-glc-(epi)catechin (T–A type)[c]	[38]
17	25.27	1087	Mv-glc-(epi)catechin-(epi)gallocatechin (A–T type)[b,c]	[38]
20	26.34	1087	Mv-glc-(epi)catechin-(epi)gallocatechin (A–T type)[b,c]	[38]
24	27.75	751	Pe-glc-(epi)catechin (T–A type)[b]	[30,31,34,38,47]
28	28.12	1087	Mv-glc-(epi)catechin-(epi)gallocatechin (A–T type)[b,c]	[38]
29	28.18	781	Mv-glc-catechin (T–A type)	[30,31,34,36,38]
32	30.03	1087	Mv-glc-(epi)catechin-(epi)gallocatechin (A–T type)[b,c]	[38]
37	30.77	1041	Pe-glc-di(epi)catechin (A–T type)[b,c]	[38]
41	31.98	1071	Mv-glc-di(epi)catechin (A–T type)[b,c]	[38]
47	33.81	1069	Mv-glc-di(epi)catechin (T–A type)[b,c]	[17,34,36,38]
49	34.52	781	Mv-glc-epicatechin (T–A type)	[30,31,34,36,38]
54	36.22	1057	Pt-glc-di(epi)catechin (A–T type)[b,c]	[38]
56	36.83	1041	Pe-glc-di(epi)catechin (A–T type)[b,c]	[38]
57	36.90	1071	Mv-glc-di(epi)catechin (A–T type)[b,c]	[38]
67	41.53	769	Pt-glc-(epi)catechin (A–T type)[b]	[38]
68	41.58	823	Mv-acetylglc-(epi)catechin[b]	[30,31]
73	43.60	799	Mv-glc-(epi)gallocatechin (A–T type)[b]	[38]
82	47.10	753	Pe-glc-(epi)catechin (A–T type)[b]	[38]
83	48.00	783	Mv-glc-(epi)catechin (A–T type)[b]	[38,49,50]
90	49.94	799	Mv-glc-(epi)gallocatechin (A–T type)[b]	[38]
101	52.78	927	Mv-coumglc-(epi)catechin (T–A type)[b]	[17]
107	55.34	753	Pe-glc-(epi)catechin (A–T type)[b]	[38]
109	56.44	783	Mv-glc-(epi)catechin (A–T type)[b]	[49,50]
Acetaldehyde-mediated tannin adducts				
70	41.97	781	Dp-glc-ethyl-catechin	[30,36]
78	45.01	781	Dp-glc-ethyl-epicatechin	[30,36]
91	49.98	825	Mv-glc-ethyl-gallocatechin	[36]
93	50.85	809	Mv-glc-ethyl-catechin	[30,31,47,51]
94	50.93	825	Mv-glc-ethyl-epigallocatechin	[36]
102	52.93	809	Mv-glc-ethyl-epicatechin	[30,31,47,51]
117	62.89	851	Mv-acetylglc-ethyl-catechin	[30]
124	66.90	955	Mv-coumglc-ethyl-catechin	[17,30,34]
126	68.14	955	Mv-coumglc-ethyl-epicatechin	[6,17,30,34]
Anthocyanin–vinylflavanol condensation products				
89	49.83	1093	Mv-glc-4-vinyl-di(epi)catechin[b,c]	[17,34,36,39]
95	51.04	1093	Mv-glc-4-vinyl-di(epi)catechin[b,c]	[17,34,36,39]
103	53.97	1135	Mv-acetylglc-vinyl-di(epi)catechin[b,c]	[36,39]
105	54.96	1135	Mv-acetylglc-vinyl-di(epi)catechin[b,c]	[36,39]
118	63.51	805	Mv-glc-vinyl-catechin	[36,39,52]
123	66.47	847	Mv-acetylglc-vinyl-catechin	[34,36]
129	69.76	805	Mv-glc-vinyl-epicatechin	[36,39,47,52]
130	70.99	951	Mv-coumglc-vinyl-catechin	[34,36,39]
131	71.64	847	Mv-acetylglc-vinyl-epicatechin	[34,36]
132	73.37	951	Mv-coumglc-vinyl-epicatechin	[34,36,39]

[a] Dp = delphinidin, Cy = cyanidin, Pt = petunidin, Pe = peonidin, Mv = malvidin, glc = glucoside, coum = coumaroyl-.
[b] Identification of proanthocyanin isomer(s) could not be established due to lack of standards.
[c] Sequence of proanthocyanidin units could not be established due to lack of standards.

the double that of conventional LC–MS methods, the improvement in separation power more than justifies a longer analysis time, as detailed in the following paragraphs.

A total of 101 anthocyanins and derived pigments were tentatively identified in a single analysis of this red wine sample (Tables 1–3). To simplify the following discussion, peak numbers specified in these tables are used throughout the text.

Seventeen grape-derived anthocyanins were identified, including the glucosides, acetyl-glucosides and coumaroyl-glucosides of cyanidin, delphinidin, petunidin, peonidin and malvidin. In addition, malvidin-(6-caffeoyl)-3-glucoside (**115**) and *cis*-malvidin-3-(p-coumaroyl)-glucoside (**121**) were also detected, the latter eluting before the much more abundant *trans* isomer [31,32]. These compounds were identified based on relative retention times and mass spectral data compared to literature reports. Aglycone fragments (loss of 162, 204 and 308 for glucosides, acetyl-glucosides and coumaroyl-glucosides, respectively) were commonly observed in the mass spectra for these compounds.

In addition, two compounds with identical mass spectra to malvidin-3-O-glucoside and malvidin-3-O-acetyl-glucoside, but eluting earlier than these compounds, were detected. These were tentatively identified as malvidin-3-O-galactoside (**51**) and malvidin-3-O-acetyl-galactoside (**81**), according to Wang et al. [33].

Especially for the grape-derived anthocyanins much sharper peaks and improved resolution is observed on the 1.7 μm column operated at optimal flow rate and 50 °C (Fig. 7). Since these compounds are the dominant pigments in young wines and as a result often obscure derived pigments, this improved resolution results in clearer mass spectra and in this manner facilitates the identification of minor pigments.

Six anthocyanidin-di-glucosides were tentatively identified based on mass spectra and relative retention times compared to [31,34]. These include the 3,5-diglucosides of delphinidin (**10**), peonidin (**33**) and malvidin (**38**), as well as the corresponding 3,7-diglucosides of peonidin (**52**) and malvidin (**58**). The latter compounds elute later than the corresponding 3,5 di-glucosides [31], although isolated peonidin-3,7-diglucoside from Garnacha Tintor-

Table 3
Pyranoanthocyanins tentatively identified in a 2-year old Pinotage wine. Peak numbers correspond to Figs. 5–8.

Peak No.	t_R (min)	[M+]	Compound[a]	Reference(s)
Anthocyanin–vinylphenol condensation products (pyranoanthocyanins)				
104	54.83	581	Dp-glc-4-vinylphenol	[30]
122	65.50	595	Pt-glc-4-vinylphenol	[30,36]
128	68.84	625	Mv-glc-vinylcatechol (Pinotin A)	[36]
133	74.23	609	Mv-glc-vinylphenol (Pigment A)	[36,39,47]
134	75.66	727	Dp-coumglc-4-vinylphenol adduct	[30]
135	76.66	639	Mv-glc-vinylguaiacol	[30,31,36]
136	79.66	651	Mv-acetylglc-vinylphenol	[36,47]
137	84.84	755	Mv-coumglc-vinylphenol (Pigment B)	[36,47]
Anthocyanin–pyruvic acid products (Vitisin A derivatives)				
34	30.04	533	Dp-glc-pyruvic acid	[36]
44	33.16	575	Dp-acetylglc-pyruvic acid	[36]
60	37.69	547	Pt-glc-pyruvic acid	[30,36,47]
66	41.01	589	Pt-acetylglc-pyruvic acid	[30,36,47]
71	42.90	531	Pe-glc-pyruvic acid	[36,47]
74	44.26	679	Dp-coumglc-pyruvic acid	[36]
76	44.54	561	Mv-glc-pyruvic acid (Visitin A)	[30,36,47]
86	48.37	573	Pe-acetylglc-pyruvic acid	[36,47]
87	48.82	603	Mv-acetylglc-pyruvic acid	[30,36,47]
97	51.80	693	Pt-coumglc-pyruvic acid	[30,36,47]
113	59.68	677	Pe-coumglc-pyruvic acid	[36,47]
114	59.97	707	Mv-coumglc-pyruvic acid	[30,36,47]
Anthocyanin–acetaldehyde derivatives (Vitisin B derivatives)				
63	39.00	489	Dp-glc-acetaldehyde	[36]
79	45.17	487	Pe-glc-acetaldehyde	[36]
80	46.34	517	Mv-glc-acetaldehyde (Visitin B)	[30,47]
96	51.78	559	Mv-acetylglc-acetaldehyde	[30,31,47]
120	64.23	663	Mv-coumglc-acetaldehyde	[36]
Anthocyanin–acetone derivatives				
92	50.46	501	Pe-glc-acetone	[30]
100	52.41	531	Mv-glc-acetone	[13,30,32,36,53]

[a] Dp = delphinidin, Cy = cyanidin, Pt = petunidin, Pe = peonidin, Mv = malvidin, glc = glucoside, coum = coumaroyl-.

era grapes has been shown to elute before peonidin-3,5-diglucoside by some authors [35]. Peak shapes for all these compounds were relatively broad, indicating that secondary equilibria equally affect the chromatographic performance of anthocyanidin-di-glucosides. Malvidin-3-coumaroyl-5-diglucoside (**111**) was also identified according to [34]. All di-glycosidic anthocyanins were present at much lower levels than the corresponding glycosidic compounds, as expected for *Vitis vinifera* cv Pinotage wines.

Oligomeric anthocyanins resulting from the direct condensation of anthocyanins were identified for the first time in grape skins

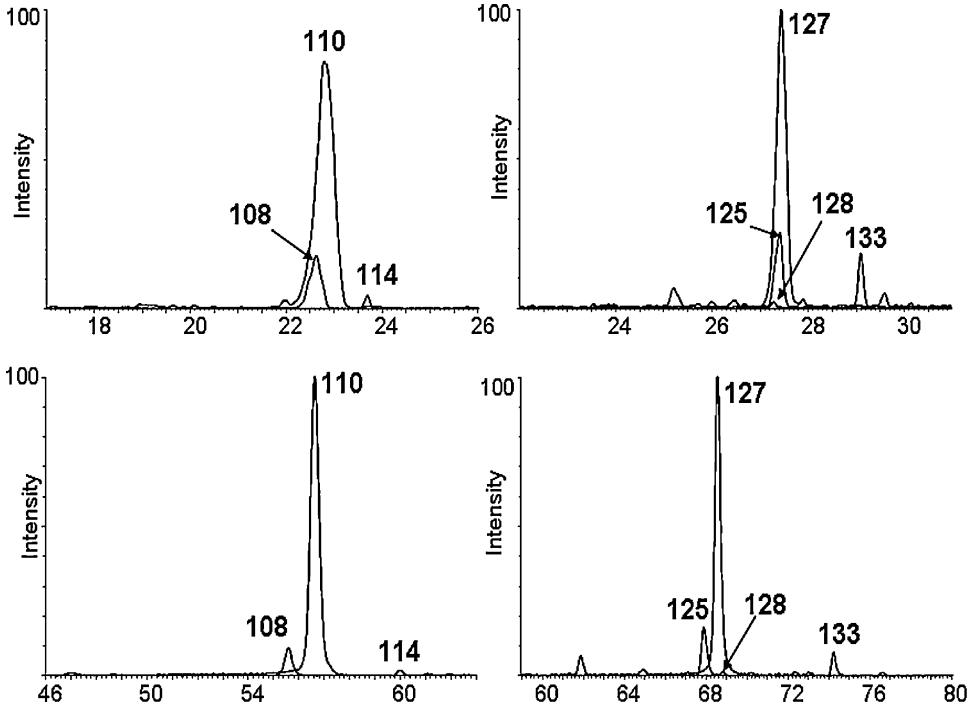

Fig. 7. Comparison of extracted ion chromatograms for the analysis of anthocyanins and derived products in red wine under conventional conditions (Top: 250 mm L × 4.6 mm I.D., 5 μm d_p column, 25 °C, 1 mL/min) and optimized conditions (Bottom: 2 mm × 100 mm L × 2.1 mm I.D., 1.7 μm d_p column, 50 °C, 0.06 mL/min). Peak numbers correspond to Tables 1–3.

Table 4
Proanthocyanins tentatively identified in a 2-year old Pinotage wine. Peak numbers correspond to Figs. 5–8.

Peak No.	t_R (min)	[M+]	Compound	Reference(s)
Proanthocyanins				
1	9.65	611	Gallocatechin-gallocatechin[a]	[41]
2	10.57	883	Trimeric prodelphinidin (GC top unit)[b,c]	[17]
3	10.68	867	Trimeric procyanidin (catechin-catechin-catechin, C2)[d]	[45]
4	13.66	867	Trimeric procyanidin (epicatechin-epicatechin-catechin)[d]	[45]
5	14.62	595	Catechin-gallocatechin[a]	[41,44]
6	15.10	595	Epicatechin-gallocatechin[a]	[41,44]
7	17.67	595	Gallocatechin-catechin[a]	[41,44]
9	21.08	1155	Tetrameric procyanidin[b]	[17]
11	21.27	883	Trimeric prodelphinidin (GC top unit)[b,c]	[17]
12	21.27	595	Gallocatechin-epicatechin[a]	[41,44]
13	23.38	1155	Tetrameric procyanidin[b]	[17]
15	24.04	883	Trimeric prodelphinidin (C top unit)[b,c]	[17]
16	24.12	579	Procyanidin B3 (dimer)[a]	[41,44]
18	26.02	1155	Tetrameric procyanidin[b]	[17]
19	26.32	867	Trimeric procyanidin (epicatechin-epicatechin-catechin)[d]	[45,54]
21	27.24	1443	Pentameric procyanidin[b]	[17]
22	27.53	867	Trimeric procyanidin (catechin-catechin-epicatechin)[d]	[45,54]
23	27.60	1155	Tetrameric procyanidin[b]	[17]
26	28.00	1443	Pentameric procyanidin[b]	[17]
27	28.10	291	Catechin	[41]
31	29.07	579	Procyanidin B1 (dimer)[a]	[17]
35	29.99	867	Trimeric procyanidin (epicatechin-epicatechin-epicatechin)[d]	[45]
36	30.06	1155	Tetrameric procyanidin[b]	[17]
39	31.04	1155	Tetrameric procyanidin[b]	[17]
40	31.32	579	Procyanidin B4 (dimer)[a]	[41,44,54]
43	32.44	1155	Tetrameric procyanidin[b]	[17]
45	33.49	883	Trimeric prodelphinidin (C top unit)[b,c]	[11,17]
46	33.67	1443	Pentameric procyanidin[b]	[17]
50	34.65	867	Trimeric procyanidin (epicatechin-epicatechin-catechin)[d]	[41,45]
53	36.03	291	Epicatechin	[41]
55	36.45	867	Trimeric procyanidin (epicatechin-epicatechin-epicatechin, C1)[d]	[41,45]
59	37.46	1115	Tetrameric procyanidin[b]	[54]
61	37.81	1443	Pentameric procyanidin[b]	[54]
62	38.74	579	Procyanidin B2 (dimer)[a]	[41,44,54]
77	44.71	867	Trimeric procyanidin [b]	[41]
85	48.25	579	Procyanidin B7/B5 (dimer)[a]	[41,44]

[a] Elution order according to [41,44,45].
[b] Sequence of proanthocyanidin units could not be established due to lack of standards.
[c] GC = (epi)gallocatechin, C = (epi)catechin.
[d] Elution order according to [45].

[7] and recently also in red wine [6] and grape extracts [36]. In the current study 7 oligomeric anthocyanins were identified based on comparison of mass spectra and relative retention times with these reports. These include dimers of malvidin-glucoside and delphinidin-glucoside (**69**), petunidin-glucoside (**75**), peonidin-glucoside (**98**) and malvidin-glucoside (**99**). Moreover, the dimers malvidin-glucoside-malvidin-coumaroyl-glucoside (**119**) and malvidin-glucoside-malvidin-acetylglucoside (**112**) and a trimeric anthocyanin resulting from the condensation of (epi)catechin with dimeric malvidin-glucoside (**30**) were also tentatively identified. All these compounds were present at trace amounts and eluted after their corresponding monomeric anthocyanins [7]. Limited fragmentation information was obtained under our conditions, although the loss of glucoside was observed for **99**.

It is relevant to note that dimeric anthocyanin-glucosides are characterised by very broad peaks in RP-LC analysis (~3 min baseline width for **99**), as reported previously [6,7], even under the improved conditions used here. This may be due to interconversion reactions similar to those described for monomeric anthocyanins, but further exacerbated in the case of dimeric anthocyanins. Peaks for the dimeric anthocyanins containing one acetyl-glucoside (**112**) or coumaroyl-glucoside (**119**) are less broad [6], supporting this hypothesis.

The derived pigments resulting from reaction of anthocyanins with proanthocyanidins identified in the Pinotage wine are summarised in Table 2. Twenty four direct tannin adducts were identified, including both anthocyanin–tannin (A–T) and tannin–anthocyanin (T–A) types. The latter condensation products are thought to occur in bicyclic form [37,38]. In accordance with previous reports [36,39], T–A adducts elute before their corresponding A–T products in RP-LC. Adducts consisting of 1 anthocyanin (petunidin-, peonidin- and malvidin-glucosides adducts were detected) and 1 or 2 units of (epi)catechin and/or (epi)gallocatechin were detected. Distinction between (epi)catechin and (epi)gallocatechin units is relatively easy based on m/z differences of 16 as well as relative retention times (gallocatechins elute before catechins in RP-LC). Note though that the exact sequence of the procyanidin moiety could not be established by LC–MS. Fragmentation observed for anthocyanin–proanthocyanin adducts includes loss of glucose (-162 m/z) from either the molecular ion or the anthocyanin fragment, proanthocyanidin units ($-m/z$ 288 for (epi)catechin) and retro-Diels–Alder fission to eliminate 152 m/z [39]. Interestingly, the T–A type adducts are characterised by relatively broad peaks compared to their A–T counterparts, indicating that the lower unit is largely responsible for the chromatographic characteristics of these adducts. This suggests an additional criterion for tentative identification of the compounds in wine samples.

Nine acetaldehyde mediated condensation products were tentatively identified based on the detection of their respective molecular ions. These contain anthocyanins (delphinidin- and malvidin-glucosides) linked via an ethyl bridge to (epi)catechin or (epi)gallocatechin – only dimeric acetaldehyde mediated adducts were detected. Differentiation of isomers is based on

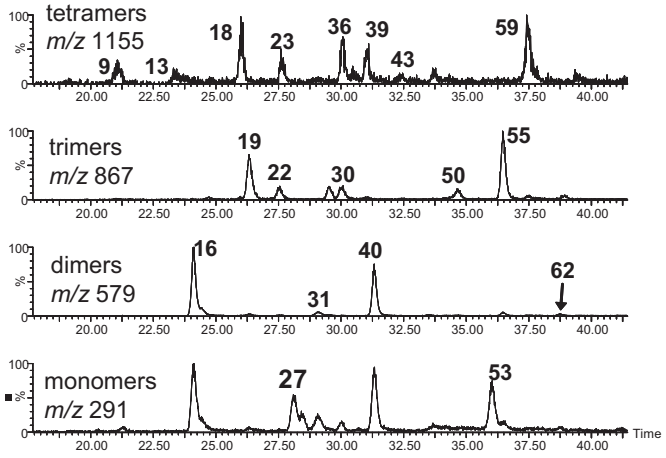

Fig. 8. Extracted ion chromatograms for the analysis of procyanidins in red wine under optimized conditions (2 mm × 100 mm L × 2.1 mm I.D., 1.7 μm d_p column, 50 °C, 0.06 mL/min). Peak numbers correspond to Table 4.

the relative retention times of catechin/epicatechin and gallocatechin/epigallocatechin.

Ten vinylflavanol condensation products were also observed, corresponding to the vinyl adducts of malvidin-glucoside (**118**, **129**), malvidin-acetyl-glucoside (**123**, **131**) and malvidin-coumaroyl-glucoside (**130**, **132**) with catechin or epicatechin. Very little fragmentation was observed for these compounds under the conditions employed here. In addition, the vinylflavanol adducts of malvidin-glucoside (**89** and **95**) and malvidin-acetyl-glucoside (**103** and **105**) with dimeric procyanidins were also observed [40].

Pyranoanthocyanins (Table 3) in wine are formed by cyclo-addition of pyruvic acid, acetaldehyde, acetone or vinylphenolds to anthocyanins. Anthocyanin-vinylphenol condensation products resulting from the reaction of cinnamic acids and anthocyanins [12] were tentatively identified in the wine sample (Table 3). In total, 8 vinylphenol derivatives were detected. These include the p-coumaric acid (vinylphenol) adducts of delphinidin-glucoside (**104**), petudin-glucoside (**122**), malvidin-glucoside (**133**), delphinidin-coumaroyl-glucoside (**134**), malvidin-acetyl-glucoside (**136**) and malvidin-coumaroyl-glucoside (**137**). Also malvidin-vinylcatechol (Pinotin A [41], **128**), resulting from a similar reaction involving caffeic acid, and malvidin-vinylguaicol (**135**) resulting from reaction with ferulic acid were detected.

The reaction between anthocyanins and pyruvic acid (the latter formed during fermentation) leads to the production of the so-called A-type vitisins. In total, 12 A-type vitisin derivatives were identified in the current study. These correspond to the pyruvic acid derivatives of delphinidin-, petunidin-, peonidin- and malvidin-glucosides (**34**, **60**, **71** and **76**), -acetylglucosides (**44**, **66**, **86** and **87**) and -coumaroylglucosides (**74**, **97**, **113** and **114**). Similarly, pyranoanthocyanins resulting from the reaction of anthocyanins and acetaldehyde (so-called B-type vitisins) were also observed. These include B-type vitisins of delphinidin (**63**)- peonidin (**79**)- and malvidin-glucosides (**80**), as well as malvidin-acetyl (**96**)- and coumaroyl-glucosides (**120**). Finally, the acetone derivatives of peonidin-glucoside (**92**) and malvidin-glucoside (**100**) were also observed in the wine sample.

In addition to the pigmented molecules, much improved separation is also observed for proanthocyanidins in the wine samples (Fig. 8). Proanthocyanidins are non-coloured oligomeric phenolic compounds composed of (epi)catechin (procyanidins) and (epi)gallocatechin (prodelphinidins) units. The improved resolution observed for procyanidins under the optimal conditions for anthocyanins is presumably due to the fact that these relatively large oligomeric compounds are characterised by low optimal flow rates under conventional conditions (due to low diffusion coefficients in the mobile phase). Therefore both the use of low flow rates and elevated temperatures are expected to result in improved separation of these compounds. Table 4 summarises the proanthocyanidins tentatively identified in the Pinotage wine sample using the optimized conditions, including 9 prodelphinidins and 27 procyanidins. No gallated proanthocyanidins were detected in the wine sample, in accordance with previous reports [42–44].

Regarding prodelphinidins, dimers and trimers containing 1 or 2 (epi)gallocatechin units were detected. It has been shown [45] that retro-Diels–Alder fragmentation of procyanidins occurs at the upper phenolic unit. This allows identification of the upper unit as either (epi)gallocatechin (loss of 168 m/z) or (epi)catechin (loss of 152 m/z). Under reversed phase conditions, the elution order of monomeric flavanols is gallocatechin < epigallocatechin < catechin < epicatechin. Accordingly, it is also clear that the retention of prodelphinidins is determined by the lower unit of oligomers [42].

Procyanidins up to a degree of polymerisation (DP) of 5 were also detected. These include 5 dimeric-, 8 trimeric-, 8 tetrameric- and 4 pentameric procyanidins. While MS does not allow identification of the sequence of flavanol building blocks, relative retention times may be used to tentatively identify dimeric and some trimeric procyanidins [42,45,46,54]. Typical fragmentation patterns for procyanidins are in accordance with [42]: both loss of (epi)catechin units (288 m/z) and RDA fission (loss of 152 m/z) are observed.

4. Conclusions

The on-column inter-conversion between anthocyanins species in the mobile phase has important implications for the optimal analysis of these compounds in RP-LC. On conventional columns operated at near-ambient temperatures and conventional flow rates, poor chromatographic efficiency results in frequent co-elution for complex samples such as red wine. This may be circumvented by using very low flow rates, implying unacceptably long analysis times. We have shown how the use of long (200 m) columns packed with small (1.7 μm) particles in combination with elevated temperature (50 °C) results in a large increase in efficiency under isocratic elution conditions. Fixed-length kinetic plots show that these gains can be achieved at conventional pressures within reasonable analysis times. Gradient separation under these conditions results in an important improvement in terms of peak capacity. Moreover, provided that certain instrumental adaptations are made to meet the requirements of small-volume columns [47], these analyses may be performed on conventional instrumentation. This approach therefore holds promise for the routine analysis of complex anthocyanin-containing samples such as red wine.

We further demonstrated how, in combination with MS detection, analysis using these optimized conditions facilitates the identification of a large number of anthocyanins and derived pigments in a red wine sample. Thus we were able to tentatively identify 101 anthocyanin derivatives (including anthocyanins, anthocyanidin-di-glucosides, oligomeric anthocyanins, pyranoanthocyanins and anthocyanin–tannin adducts) and 36 proanthocyanidins in a single analysis. Improved analytical methods for the determination of especially minor anthocyanin derivatives are of interest for the in-depth investigation of these important natural pigments in a variety of natural products, not least of which red wine.

Acknowledgements

The authors gratefully acknowledge Kathithileni M. Kalili for experimental assistance, and Stellenbosch University, the Third

World Academy of Science (TWAS, 08-077 RG/CHE/AF/AC), the International Foundation of Science, Stockholm, Sweden (IFS, F/4904-1, AdV) and the National Research Foundation (NRF, South Africa) for financial support. D. Cabooter is a Fellow of the Research Foundation Flanders (FWO).

References

[1] J.B. Harborne, The Flavonoids, Advances in Research Since 1986, CRC Press, London, 1999.
[2] G. Mazza, R. Brouillard, Food Chem. 25 (1987) 207.
[3] A. Castaneda-Ovando, M.d.L. Pacheco-Hernandez, M.E. Paez-Hernandez, J.A. Rodriguez, C.A. Galon-Vidal, Food Chem. 113 (2009) 859.
[4] S. Remy, H. Fulcrand, B. Labarbe, V. Cheynier, M. Moutounet, J. Sci. Food Agric. 80 (2000) 745.
[5] H. Fulcrand, T. Doco, N.-E. Es-Safi, V. Cheynier, M. Moutounet, J. Chromatogr. A 752 (1996) 85.
[6] C. Alcalde-Eon, M.T. Escribano-Bailon, C. Santos-Buelga, J.C. Rivas-Gonzalo, J. Mass Spectrom. 42 (2007) 735.
[7] S. Vidal, E. Meudec, V. Cheynier, G. Skouroumounis, Y. Hayasaka, J. Agric. Food Chem. 52 (2004) 7144.
[8] J. Bakker, C.F. Timberlake, J. Agric. Food Chem. 45 (1997) 35.
[9] J. Bakker, P. Bridle, T. Honda, H. Kuwano, N. Saito, N. Terahara, C.F. Timberlake, Phytochemistry 44 (1997) 1375.
[10] H. Fulcrand, C. Benabdeljalil, J. Rigaud, V. Cheynier, M. Moutounet, Phytochemistry 47 (1998) 1401.
[11] H. Fulcrand, P.J. Cameira Dos Santos, P. Sarni-Manchado, V. Cheynier, J. Favre-Bonvin, J. Chem. Soc. Perkin Trans. 1 (1996) 735.
[12] M. Schwarz, T.C. Wabnitz, P. Winterhalter, J. Agric. Food Chem. 51 (2003) 3682.
[13] J. He, C. Santos-Buelga, A.M.S. Silva, N. Mateus, V. deFreitas, J. Agric. Food Chem. 54 (2006) 9598.
[14] E.M. Francia-Aricha, M.T. Guerra, J.C. Rivas-Gonzalo, C. Santos-Buelga, J. Agric. Food Chem. 45 (1997) 2262.
[15] J.C. Rivas-Gonzalo, S. Bravo-Haro, C. Santos-Buelga, J. Agric. Food Chem. 43 (1995) 1444.
[16] N. Mateus, A.M.S. Silva, J.C. Rivas-Gonzalo, C. Santos-Buelga, V. De Freitas, J. Agric. Food Chem. 51 (2003) 1919.
[17] C. Vergara, C. Mardones, I. Hermosín-Gutiérrez, D. von Baer, J. Chromatogr. A (2010) 5710.
[18] B. Sun, M.C. Leandro, V. de Freitas, M.I. Spranger, J. Chromatogr. A 1128 (2006) 27.
[19] A. de Villiers, D. Cabooter, F. Lynen, G. Desmet, P. Sandra, J. Chromatogr. A 1216 (2009) 3270.
[20] G. Desmet, D. Clicq, P. Gzil, Anal. Chem. 77 (2005) 4058.
[21] A. de Villiers, F. Lynen, P. Sandra, J. Chromatogr. A 1216 (2009) 3431.
[22] H. Chen, C. Horváth, Anal. Methods Instrum. 1 (1993) 213.
[23] C.R. Wilke, P. Chang, AIChE J. 1 (1955) 264.
[24] G. Desmet, D. Cabooter, P. Gzil, H. Verelst, D. Mangelings, Y.V. Heyden, D. Clicq, J. Chromatogr. A 1130 (2006) 158.
[25] A. de Villiers, H. Lauer, R. Szucs, S. Goodall, P. Sandra, J. Chromatogr. A 1113 (2006) 84.
[26] G. Desmet, D. Clicq, D.T.T. Nguyen, D. Guillarme, S. Rudaz, J.L. Veuthey, N. Vervoort, G. Torok, D. Cabooter, P. Gzil, Anal. Chem. 78 (2006) 2150.
[27] X. Wang, W.E. Barber, P.W. Carr, J. Chromatogr. A 1107 (2006) 139.
[28] K. Broeckhoven, D. Cabooter, F. Lynen, P. Sandra, G. Desmet, J. Chromatogr. A 1217 (2010) 2787.
[29] D. Cabooter, A. de Villiers, D. Clicq, R. Szucs, P. Sandra, G. Desmet, J. Chromatogr. A 1147 (2007) 183.
[30] U.D. Neue, J. Chromatogr. A 1079 (2005) 153.
[31] C. Alcalde-Eon, M.T. Escribano-Bailon, C. Santos-Buelga, J.C. Rivas-Gonzalo, Anal. Chim. Acta 563 (2006) 238.
[32] E. Boido, C. Alcalde-Eon, F. Carrau, E. Dellacassa, J.C. Rivas-Gonzalo, J. Agric. Food Chem. 54 (2006) 6692.
[33] H. Wang, E.J. Race, A.J. Shrikhande, J. Agric. Food Chem. 51 (2003) 7989.
[34] H. Wang, E.J. Race, A.J. Shrikhande, J. Agric. Food Chem. 51 (2003) 1839.
[35] N. Castillo-Munoz, P. Winterhalter, F. Weber, M.V. Gomez, S. Gomez-Alonso, E. Garica-Romero, I. Hermosin-Guierrez, J. Agric. Food Chem. 58 (2010) 11105.
[36] S. Pati, I. Losito, G. Gambacorta, E.L. Notte, F. Palmisano, P.G. Zambonin, J. Mass Spectrom. 41 (2006) 861.
[37] M. Monagas, B. Bartolomé, C. Gómez-Cordovés, Crit. Rev. Food Sci. Nutr. 45 (2005) 85.
[38] S. Remy-Tanneau, C. Le Guerneve, E. Meudec, V. Cheynier, J. Agric. Food Chem. 51 (2003) 3592.
[39] Y. Hayasaka, J.A. Kennedy, Aust. J. Grape Wine Res. 9 (2003) 210.
[40] J. He, C. Santos-Buelga, N. Mateus, V. de Freitas, J. Chromatogr. A 1134 (2006) 215.
[41] M. Schwarz, G. Jerz, P. Winterhalter, Vitis 42 (2003) 105.
[42] S. Pascual-Teresa, J.C. Rivas-Gonzalo, C. Santos-Buelga, Int. J. Food Sci. Technol. 35 (2000) 33.
[43] H. Fulcrand, S. Remy, J.-M. Souquet, V. Cheynier, M. Moutounet, J. Agric. Food Chem. 47 (1999) 1023.
[44] S.A. Lazarus, G.E. Adamson, J.F. Hammerstone, H.H. Schmitz, J. Agric. Food Chem. 47 (1999) 3693.
[45] C. Santos-Buelga, C. Garcia-Viguera, F.A. Tomas-Barberan, in: C. Santos-Buelga, G. Williamson (Eds.), Methods in Polyphenol Analysis, The Royal Society of Chemistry, Cambridge, 2003, p. 92.
[46] C. Santos-Buelga, E.M. Francia-Aricha, M.T. Escribano-Bailón, Food Chem. 53 (1995) 197.
[47] F. Gritti, C.A. Sanchez, T. Farkas, G. Guiochon, J. Chromatogr. A 1217 (2010) 3000.
[48] A. de Villiers, G. Vanhoenacker, P. Majek, P. Sandra, J. Chromatogr. A 1054 (2004) 195.
[49] S. Pati, M.T. Liberatore, G. Gambacorta, D. Antonacci, E. La Notte, J. Chromatogr. A 1216 (2009) 3864.
[50] B. Sun, C.P. Reis Santos, M.C. Leandro, V. De Freitas, M.I. Spranger, Rapid Commun. Mass Spectrom. 21 (2007) 2227.
[51] M. Mirabel, C. Saucier, C. Guerra, Y. Glories, Am. J. Enol. Vitic. 50 (1999) 211.
[52] N. Mateus, A.M.S. Silva, C. Santos-Buelga, J.C. Rivas-Gonzalo, V. de Freitas, J. Agric. Food Chem. 50 (2002) 2110.
[53] Y. Lu, L.Y. Foo, Tetrahedron Lett. 42 (2001) 1371.
[54] J.C. Hufnagel, T. Hofmann, J. Agric. Food Chem. 56 (2008) 1376.